

# A Semiconducting Two-Dimensional Polymer as an Organic Electrochemical Transistor Active Layer

Reem B. Rashid, Austin M. Evans, Lyndon A. Hall, Raghunath R. Dasari, Emily K. Roesner, Seth R. Marder, Deanna M. D'Allesandro, William R. Dichtel,\* and Jonathan Rivnay\*

Organic electrochemical transistors (OECTs) are devices with broad potential in bioelectronic sensing, circuits, and neuromorphic hardware. Their unique properties arise from the use of organic mixed ionic/electronic conductors (OMIECs) as the active channel. Typical OMIECs are linear polymers, where defined and controlled microstructure/morphology, and reliable characterization of transport and charging can be elusive. Semiconducting two-dimensional polymers (2DPs) present a new avenue in OMIEC materials development, enabling electronic transport along with precise control of well-defined channels ideal for ion transport/intercalation. To this end, a recently reported 2DP, TIIP, is synthesized and patterned at 10  $\mu\text{m}$  resolution as the channel of a transistor. The TIIP films demonstrate textured microstructure and show semiconducting properties with accessible oxidation states. Operating in an aqueous electrolyte, the 2DP-OECT exhibits a device-scale hole mobility of  $0.05 \text{ cm}^2 \text{ V}^{-1} \text{ s}^{-1}$  and a  $\mu\text{C}^*$  figure of merit of  $1.75 \text{ F cm}^{-1} \text{ V}^{-1} \text{ s}^{-1}$ . 2DP OMIECs thus offer new synthetic degrees of freedom to control OECT performance and may enable additional opportunities such as ion selectivity or improved stability through reduced morphological modulation during device operation.


## 1. Introduction

Organic electrochemical transistors (OECTs) are semiconductor-based devices that are promising for applications such as biointerfaced electronics, chemical sensing, and neuromorphic computing.<sup>[1–7]</sup> OECTs operate by transducing a gate voltage potential into a differential current between a source and drain terminal.<sup>[1,8]</sup> In an OECT architecture, the gate potential controls the bulk conductivity of the organic transistor channel by modulating the redox state of the semiconducting polymer via injection or transport of ions and charge compensation (Figure 1b,c,d).<sup>[9]</sup> Changes in bulk conductivity due to ionic doping lead to efficient ionic-to-electronic signal transduction.<sup>[1,3]</sup> To meet the demands of effective electronic transport, ionic injection and transport, and high volumetric capacitance conjugated materials called organic mixed ionic/electronic

R. B. Rashid, J. Rivnay  
Dept. of Biomedical Engineering  
Northwestern University  
Evanston, IL 60208, USA  
E-mail: jrivnay@northwestern.edu

R. B. Rashid, J. Rivnay  
Simpson Querrey Institute  
Northwestern University  
Chicago, IL 60611, USA

A. M. Evans, E. K. Roesner, W. R. Dichtel  
Department of Chemistry  
Northwestern University  
Evanston, IL 60208, USA  
E-mail: wdichtel@northwestern.edu

 The ORCID identification number(s) for the author(s) of this article can be found under <https://doi.org/10.1002/adma.202110703>.

© 2022 The Authors. Advanced Materials published by Wiley-VCH GmbH. This is an open access article under the terms of the Creative Commons Attribution-NonCommercial License, which permits use, distribution and reproduction in any medium, provided the original work is properly cited and is not used for commercial purposes.

DOI: 10.1002/adma.202110703

L. A. Hall, D. M. D'Allesandro  
School of Chemistry  
The University of Sydney  
Sydney, NSW 2006, Australia

R. R. Dasari, S. R. Marder  
School of Chemistry and Biochemistry  
Georgia Institute of Technology  
Atlanta, GA 30332, USA

S. R. Marder  
University of Colorado Boulder  
Renewable and Sustainable Energy Institute  
Boulder, CO 80303, USA

S. R. Marder  
National Renewable Energy Laboratory  
Chemistry and Nanoscience Center  
Golden, CO 80401, USA

S. R. Marder  
University of Colorado Boulder  
Department of Chemical and Biological Engineering  
Boulder, CO 80303, USA

S. R. Marder  
University of Colorado Boulder  
Department of Chemistry  
Boulder, CO 80303, USA

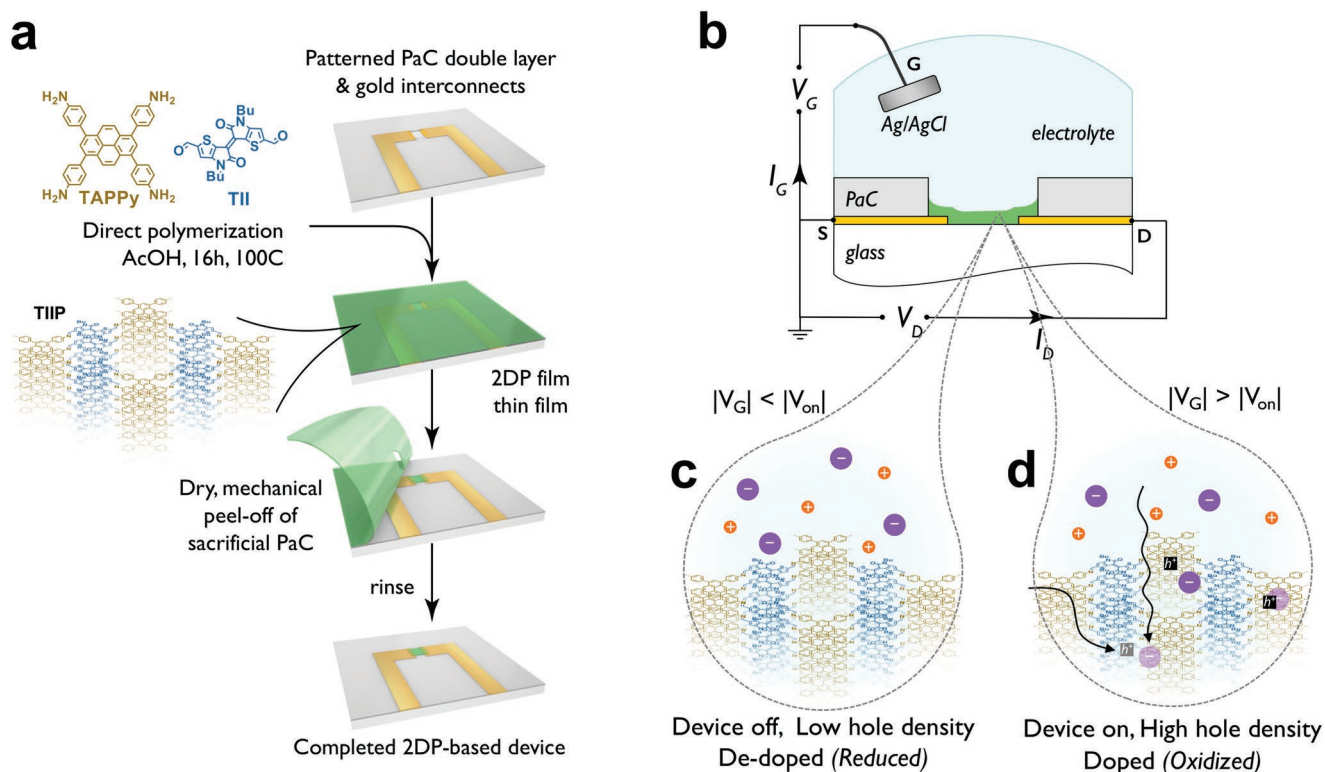


**Figure 1.** Two-dimensional polymer (2DP) transistor patterning and operation. a) TIIP direct polymerization and patterning by dry peel-off to produce transistor structures. b) OECT cross-section and modulation of conductance state between c) de-doped, when the device is off, and d) doped, when the device is on.

conductors (OMIECs) have been developed.<sup>[10,11]</sup> OMIECs are typically linear polymers or small molecules that can be polyelectrolyte doped, p-dopable, or n-dopable structures.<sup>[5,11–19]</sup> To be useful within an OECT, the OMIEC's synthetic design, microstructure, and macroscale fabrication must be optimized simultaneously to achieve high charge-carrier mobility, high ion permeability, long-term chemical stability, and fast response time.<sup>[8,20–24]</sup> To date, broadly applicable structure–property relationships for OECT materials have remained elusive due to the challenges related to unambiguously and simultaneously resolving polymer microstructure, ion injection processes, and electronic performance, especially during device operation.<sup>[11,25]</sup> In particular, conjugated polymers adapted for mixed conduction often rely on amorphous regions, ion transporting regions, porous/fibrous microstructures, or structural rearrangement such as lamellar intercalation to enable intimate ionic–electronic interactions.<sup>[10,11,22]</sup> As such, exploring OMIECs with well-defined molecular arrangements to enhance ionic and electronic transport pathways is a promising route to establish structure–performance relationships and ultimately develop new classes of OMIEC active materials.

Two-dimensional polymers (2DPs), especially those prepared from solution polymerizations known as covalent organic frameworks (COFs), have substantial potential to address limitations that exist with current OMIECs, which could lead to new material design strategies and improved OECT performance. For example, periodic chemical lattices produced by covalently cross-linking monomer subunits allow for the systematic design of polymer

microstructure. Moreover, the densely cross-linked nature of 2DPs means that their intracrystallite structure is unlikely to evolve over time, during swelling, or under device operation, which reduces concern over deteriorating device performance due to structural changes and simplifies fundamental structure–property studies.<sup>[26]</sup> This improved stability may ultimately result in more stable long-term device performance and more meaningful fundamental structure–property studies. Periodic 2DPs also contain well-defined channels that can act as conduits for ions to intercalate throughout the material. This large permanent porosity could, in principle, lead to rapid response times and high ion storage densities.<sup>[27]</sup> Moreover, precise synthetic control of nanoporous covalent networks could lead to the ion selectivities required for OECT-based sensing.<sup>[28]</sup> The advantageous structural features and demonstrated chemical versatility of macromolecular sheets inspire this interrogation of 2DP-based OECTs.

While 2DPs have attracted significant interest as organic semiconductors in various device contexts, contemporary exploration of 2DP semiconductors has been limited, with few examples showing materials capable of demonstrating practical, operational devices.<sup>[29–33]</sup> This limitation primarily arises from the poor chemical stability and low intrinsic conductivity of the boron-based 2DP systems that dominate these studies. Recently, an intrinsically semiconducting 2DP system, TIIP, was reported with bulk conductivities of  $3.5 \times 10^{-5} \text{ S m}^{-1}$  as a thin film without intentional doping,<sup>[21]</sup> along with reasonable stability in aqueous solutions. These attributes suggest that this material may be suitable for use as an OECT active layer.

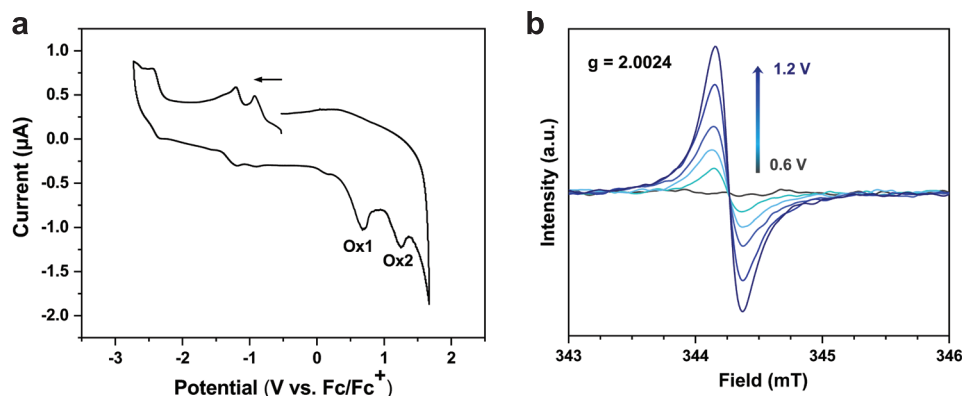


**Figure 2.** Oxidative accessibility of TIIP. a) Cyclic voltammogram of TIIP at  $100 \text{ mV s}^{-1}$  swept in the reductive direction first showing two oxidative processes. b) Electron spin resonance spectroelectrochemistry of TIIP from +0.6 to +1.2 V showing the formation of a radical upon oxidation. Experiments were conducted at room temperature in a  $0.1 \text{ M TBAPF}_6/\text{MeCN}$  electrolyte.

In addition to chemical design constraints that limit the number of semiconducting 2DPs, fabrication procedures to selectively deposit high quality, oriented, uncontaminated 2DP films in relevant device architectures are still under development. This challenge is interrelated to those associated with controlling the chemical and microstructural features of 2DP films. Recent examples of interfacial, direct-growth, or additive manufacturing film production exemplify that high-quality 2DP films are rapidly becoming available.<sup>[21,28,34–39]</sup> However, micrometer-scale patterning needed for arrays of sensors or circuits, especially in conjunction with metallic contacts, interconnects, and insulation has not been readily achieved.

Here, we produce textured thin films of the previously reported semiconducting 2DP, TIIP, which is produced by imine condensation of *N,N'*-dibutyl-6,6'-diformylthienoindigo and 1,3,6,8-tetra(aminophenyl)pyrene (Figure 1a). Through a combination of spectroscopic and electrochemical techniques, we demonstrate that TIIP is intrinsically semiconducting with addressable oxidative potentials. We then developed film synthesis conditions and microfabrication techniques to deposit micrometer-resolution TIIP films with metal interconnects and insulation to obtain 2DP-coated electrodes and OECTs with semiconducting 2DP transistor channels. Such film assembly and device fabrication showed that TIIP enables a volumetric charge ( $C^*$ ) of  $32 \text{ F cm}^{-3}$ , on par with prototypical conducting polymer OMIECs.<sup>[40]</sup> The performance of OECT devices based on TIIP active layers revealed a modest peak transconductance ( $g_m$ ) of  $0.14 \text{ S cm}^{-1}$ , a  $\mu C^*$  of  $1.75 \text{ F cm}^{-1} \text{ V}^{-1} \text{ s}^{-1}$ , and allowed for a device-scale mobility determination of  $0.05 \text{ cm}^2 \text{ V}^{-1} \text{ s}^{-1}$ . These advances in patterning 2DPs and characterizing their performance in electrochemical devices will enable broader investigations of the optoelectronic properties of this emerging macromolecular architecture.

## 2. Results and Discussion

To investigate TIIP-based OECTs, we first developed synthetic conditions to produce homogenous TIIP thin films. We prepared an electron-deficient monomer, *N,N'*-dibutyl-6,6'-diformylthienoindigo (TII), and an electron-rich monomer,

1,3,6,8-tetrakis(4-aminophenyl)pyrene (TAPPy), using previously reported methods (Scheme S1, S2, Supporting Information).<sup>[21]</sup> Next, we explored polymerization conditions to obtain TIIP as a homogenous thin film. After optimization, we found that immersing a glass substrate into the solvothermal polymerization of TAPPy ( $5 \times 10^{-3} \text{ M}$ , 1.0 equiv) and TII ( $10 \times 10^{-3} \text{ M}$ , 2.0 equiv) in a mixture of *o*-dichlorobenzene:*n*-butanol:mesitylene:acetic acid:water (20:20:2:1:1 v/v/v) at  $100 \text{ }^\circ\text{C}$  for 72 hours produced a crystalline, imine-linked 2DP films, as previously shown,<sup>[21]</sup> and confirmed below.

A series of spectroscopic measurements confirm that TIIP has the required redox accessibility needed for OECT active layers. Due to synthetic incompatibilities of our harsh synthetic protocols with the transparent conductive indium tin oxide electrodes needed for spectroelectrochemistry (SEC), we first studied polycrystalline 2DP powders that are formed concomitantly with the high-quality films produced during the solvothermal synthesis. Diffuse reflectance UV-vis spectroscopy reveals that TIIP powders have an optical absorption onset of  $850 \text{ nm}$  (Figure S1, Supporting Information), consistent with our previous observations and the pronounced emerald color of the conformal films (Figure S3, Supporting Information). Cyclic voltammetry reveals that TIIP undergoes two one-electron oxidations at +0.6 V and +1.25 V (versus  $\text{Fc}/\text{Fc}^+$ ), respectively (Figure 2a). The irreversibility of these oxidative features is likely due to the poor adhesion of oxidized TIIP to the conductive carbon used to perform this measurement, this is in contrast to the reversibility and low hysteresis of the devices presented herein. We do not consider the reductive features of this 2DP because the reductive doping of this material is unlikely to be stable under the conditions of OECT operation (e.g., ambient atmosphere). Electron spin resonance (ESR) SEC collected during an oxidative sweep showed the formation of a paramagnetic species at 0.8 V (versus  $\text{Ag}/\text{Ag}^+$ ) with a  $g$  value of 2.0024, consistent with the formation of an organic radical (Figure 2b). As the oxidative bias is swept between 0.8 V to 1.2 V the intensity of this ESR signal increases, showing that applying an oxidative bias leads to hole injection into the TIIP. These electrochemical and spectroscopic data demonstrate that TIIP has accessible redox potentials that are needed for OECT performance.

Having identified suitable polymerization conditions for TIIP and verified its redox addressability, we patterned the 2DP along with metal interconnects/electrodes and polymer insulation by applying photolithographic techniques (Figure 1a)<sup>[41]</sup> based on methods developed for patterning of living and sensitive biological soft matter. This approach features a dry peel-off process that can simultaneously define both the insulation and active polymer layer without exposure to solvents, resists, or plasmas typical of most foundry processes. First, 100 nm-thick gold interconnects and electrodes were deposited and patterned onto a glass substrate using electron beam evaporation (see Supporting Information for a full description of electrode deposition). A 2  $\mu\text{m}$ -thick layer of patterned Parylene C (PaC) with an anti-adhesive top layer was deposited on top of the patterned substrate. A second, sacrificial PaC was then deposited, and subsequently etched to define areas where the growth of the 2DP was desired. This heterostructured substrate was then immersed into a monomer-containing solution and subjected to polymerization conditions. The TIIP polymer films were washed with and then immersed into a solution of *o*-dichlorobenzene:*n*-butanol:mesitylene (5:5:2 v/v/v) and bath sonicated to remove unreacted monomers, residual oligomers, and catalysts. These films were then immersed into *n*-butanol, then methanol, and finally were dried using supercritical CO<sub>2</sub> to remove organic solvents. Following this protocol, optically uniform and transparent green TIIP films (Figure S3, Supporting Information) were produced on top of the patterned PaC multilayer stack, which appeared unperturbed. After film formation over the entire substrate, the sacrificial PaC was mechanically peeled, taking with it excess TIIP film, and leaving completed electrode and OECT structures with TIIP films of well-defined dimensions (Figure 1a, S4, Supporting Information). The resulting films show uniform coverage, with sparse, inhomogeneous particulate residue owing to the film formation process resulting in overall film root mean squared roughness of 18–88 nm (Figure S5, Supporting Information).

With few examples of patterned 2DPs for micrometer-scale devices, we first confirmed that the polymerized TIIP films formed and patterned as described above were comparable to those previously reported,<sup>[21]</sup> or those formed on isolated films on glass. The optically homogenous TIIP films polymerized

by this method are of high quality, with strong preferentially oriented structural periodicity and a high degree of chemical purity. After the polymerization, Fourier transform infrared (FT-IR) spectroscopy of the TIIP film revealed that the reactive monomer functionalities were decreased. Specifically, the amine stretches (3340 cm<sup>-1</sup>) of TAPPy and the aldehyde stretches of TII (1650 cm<sup>-1</sup>) were both substantially diminished in the TIIP film. Additionally, increased intensity centered at 1680 cm<sup>-1</sup> revealed that TIIP contains C=N bonds associated with the desired imine polymerization chemistry and is consistent with previous reports of imine-linked 2DPs.<sup>[21]</sup> As seen in the two-dimensional X-ray diffraction profile, scattering features are observed at 0.21, 0.31, 0.43, and 0.58  $\text{\AA}^{-1}$  corresponding to the 100, 110, 200, and 210 scattering vectors (Figure 3b,d). These features correspond well to the simulated scattering profile of an orthorhombic unit cell (Figure 3e) of TIIP with in-plane unit cell dimensions of 30  $\text{\AA}$  (Figure 3a,d). The scattering of the 100 diffraction feature (0.21  $\text{\AA}^{-1}$ ) is radially anisotropic, with the majority of the scattering intensity confined to the  $Q_{xy}$  axis (0° and 180°) (Figure 3c). Collectively, these data demonstrate that the TIIP films formed on the patterned multilayer PaC/glass substrates are of high quality, with a high degree of polymerization, crystallinity, and a preferential crystallite orientation with the stacking direction perpendicular to the substrate.

To evaluate electrical and electrochemical properties of patterned TIIP films, we investigated aqueous electrolyte-gated devices. Polymer-coated microelectrodes are useful for characterizing the electrochemical properties of TIIP in a form factor most relevant to OECTs. Electrochemical impedance spectroscopy of a TIIP-coated electrode operating in  $100 \times 10^{-3}$  M NaCl was used to extract capacitance. The impedance spectra were fit to a circuit model consisting of a resistor in series with a resistor and constant phase element (CPE) in parallel ( $R_s(R||C)$ ) (Figure 4a). While the impedance spectra did not fit a circuit model consisting of ideal elements as other OECT materials do, a CPE is commonly used to describe porous materials.<sup>[42]</sup> We use a constant phase element (CPE) to improve the model fit of the electrochemical impedance. Typical of nanoporous film electrodes, the CPE, or alternatively, more complex transmission line models, are often used describe anomalous diffusion,

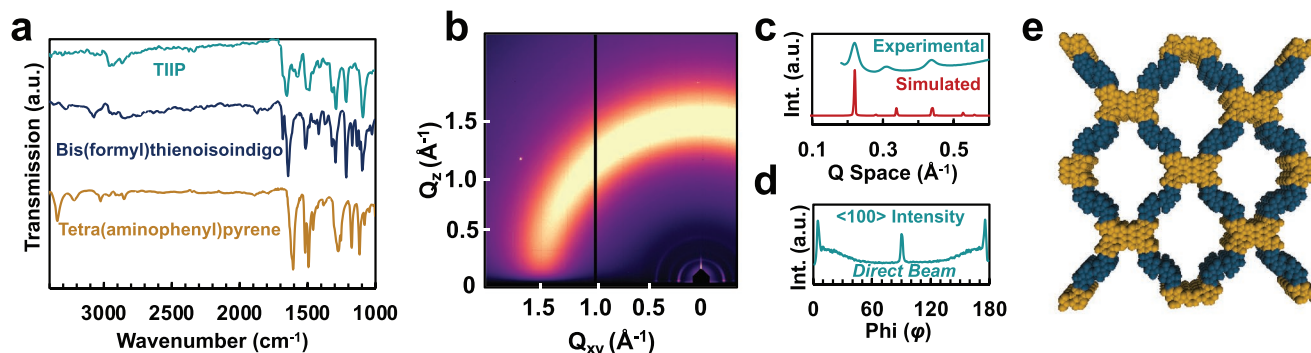


**Figure 3.** Characterization of TIIP films on devices. a) Infrared spectroscopy of TIIP and its constituent monomers. b) 2D grazing-incidence wide-angle X-ray diffraction pattern of TIIP following removal of the Parylene C layer. Note, the broad, isotropic scattering centered at  $\approx 1.5 \text{\AA}^{-1}$  is attributed to the amorphous scattering of the underlying substrate. c) Comparison of the simulated and experimental 1D X-ray scattering profile. d) Radial distribution of the <100> diffraction feature. e) Proposed structure of TIIP with tetraphenylpyrene nodes shown in gold and thienoisindigo units shown in teal.

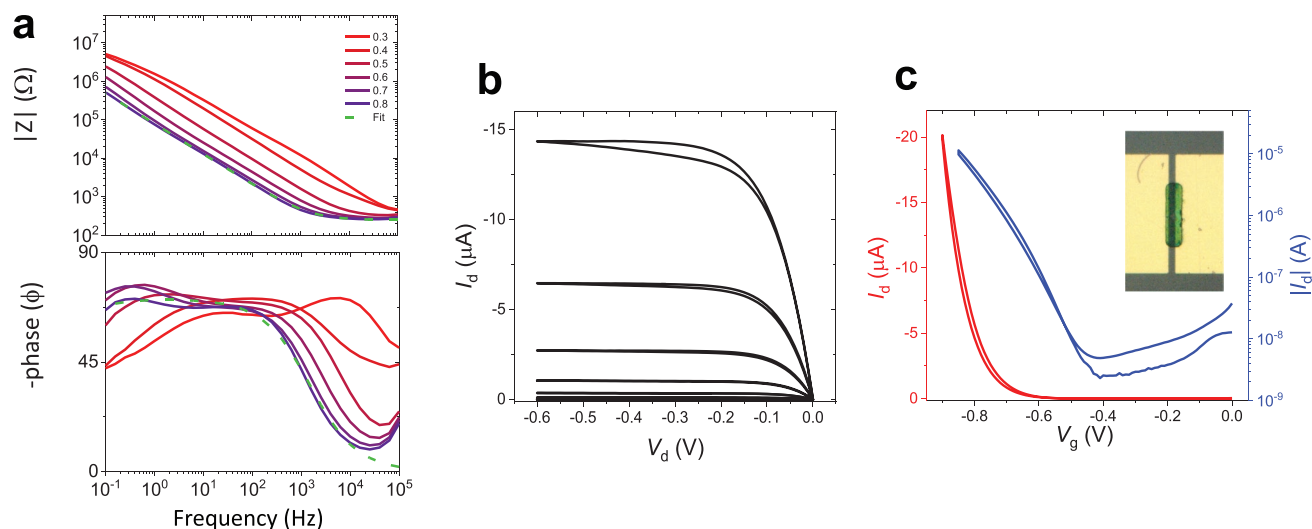


**Figure 4.** Aqueous operation of TIIP electronic devices. a) Electrochemical impedance spectroscopy of TIIP-coated electrodes at potential offsets of 0.3 to 0.8 V versus Ag/AgCl. The dotted green fits are from  $(R_s(R_p||Q))$ , which makes use of a constant phase element (Q). A pseudocapacitance was extracted from the circuit leading to a fit of  $R_s = 246 \Omega$ ,  $R_p = 8.9 M\Omega$ , and  $C = 7.1 \mu F$  b) Output curve ( $\Delta V_g = 0.05$  V, 0 V to  $-0.8$  V and  $V_d$ : 0 to  $-0.4$  V at  $0.02 V_d s^{-1}$ ) of an OECT. c) Transfer curve ( $\Delta V_g = 0.01$  V, 0 V to  $-0.8$  V at  $0.02 V_g s^{-1}$  and  $V_d = -0.4$  V) on a log and linear scale of a TIIP OECT. OECT characteristics of a  $100 \mu m \times 10 \mu m$  ( $W \times L$ ) device,  $\approx 300$  nm thick. Inset: Optical microscopy image of the TIIP OECT described above.

which cannot be described using a pure capacitor.<sup>[43]</sup> A pseudocapacitance was extracted from the CPE using  $Y_0^{(1/n)} R^{(1/n)-1}$  where  $Y_0 = 2.96 \mu S^n$  and  $n = 0.79$ . This approach yielded a value of  $0.8 \text{ mF cm}^{-2}$  at 0.8 V and showed a 20-fold increase in effective capacitance when switching the gate bias from the neutral to the oxidized state. These data suggest that the film charging is not limited to the electrolyte–TIIP interface, and that the bulk of the 2DP participates in electrochemical charging, consistent with OMIECs used in electrolyte-gated devices. Assuming the full thickness of the TIIP allows for film oxidation at these biases, the effective volumetric capacitance ( $C^*$ ) of the TIIP films would be  $32 \text{ F cm}^{-3}$  at 0.8 V. Since the uniformity of charging within the film, both in the bulk, and as a function of penetration depth, is not well explored, this reported  $C^*$  value might increase as polymerization and fabrication methods improve. Nevertheless, this  $C^*$  value is on par with other OECT materials such as the prototypical conducting polymer PEDOT:PSS, and lower than homopolymer OMIECs.<sup>[20,44]</sup> We approximate the theoretical  $C^*$  of our films by first assuming that this value will be limited by ion intercalation. From crystallographic models, we extract a unit cell volume of  $5228 \text{ \AA}^3$ . Assuming that between 2–4 charges can exist within a single unit cell (limited by pore free volume for ionic insertion), we determine that the charge density is roughly  $3.8\text{--}7.7 \times 10^{20} \text{ cm}^{-3}$ . Using previously derived relationships, we estimate that the theoretical  $C^*$  is  $73\text{--}92 \text{ F cm}^{-3}$ . Therefore, our measured  $C^*$  is approximately one-third of its theoretical potential.<sup>[45]</sup>

The output and transfer characteristics shown in Figure 4b,c are p-type (hole transport) operation ( $V_g, V_d < 0$  V), which is consistent with the findings of the ESR-SEC. The output curve shows clear linear and saturation regimes typical of transistor operation. TIIP OECTs demonstrated a normalized peak transconductance ( $g_m$ ) of  $0.14 \text{ S cm}^{-1}$  at  $-0.8$  V, which was extracted from the slope of the transfer curve ( $\delta I_d / \delta V_g$ ). The threshold voltage ( $V_{th} = 0.71$  V) was extracted from the

extrapolation of the linear regime of the  $\sqrt{|I_D|}$  versus  $V_g$  plot. Electronic mobility ( $\mu_e$ ) was then extracted using the equation  $g_m = \frac{wd}{L} \mu C^* (V_g - V_{th})$  and was  $0.05 \text{ cm}^2 \text{ V}^{-1} \text{ s}^{-1}$ . This results in a  $\mu C^*$  (OECT figure of merit) of  $1.75 \text{ F V}^{-1} \text{ cm}^{-1} \text{ s}^{-1}$ . Lastly, the shelf stability of the 2DP OECT was tested by taking transfer curves about 1 year apart. The drain current decreased from about  $12 \mu A$  to  $0.25 \mu A$  (Figure S6, Supporting Information), showing poor longevity. In benchmarking TIIP against existing OMIEC-channel materials used in OECTs, the present devices exhibit a modest figure of merit values. Top performing p-type polymer OECT materials achieve  $\mu C^* > 100 \text{ F V}^{-1} \text{ cm}^{-1} \text{ s}^{-1}$ , but the performance of TIIP is on par with the best n-type OECT active materials, which will likely be the limiting device in future circuits. With its more crystalline morphology, it may be more appropriate to compare 2DPs with crystalline small-molecule OMIECs (or potential assemblies of 2D materials) rather than linear polymers. From this perspective, TIIP outperforms or performs similarly to other crystalline OECT materials such as small molecule materials and composites; for example, a small molecule n-type fullerene-based OMIEC demonstrated a  $\mu C^*$  of  $7 \text{ F V}^{-1} \text{ cm}^{-1} \text{ s}^{-1}$ , which is within a factor of four of the TIIP OMIEC performance presented here.<sup>[14,18]</sup> 2DP-based OMIECs may indeed fill a critical gap in the field: providing a synthetic design strategy to combine the advantages of small molecule OMIECs (including precision chemical control and crystalline ordering) with the more established high performance of linear polymer-based OMIECs. Currently, TIIP shows mobility  $\approx 20$  times lower than top performing linear polymers, which could be readily improved with advances in thin-film formation and processing. However, the higher volumetric capacitances are the main reason linear polymers outperform TIIP. This may likely be due to facile ion intercalation from amorphous regimes into semicrystalline pathways, however, 2DPs or COFs have the potential for enhanced ion transport due to their

porous architecture and synthetic tunability thereof. It should be noted that the hydrophobic nature of TIIP is not ideal for the aqueous operation targeted here and may be a leading cause limiting the volumetric capacitance. However, TIIP was chosen as a proof-of-concept for 2DP OECTs as it has been previously reported, and its non-trivial in situ polymerization/film formation has already been established.<sup>[21]</sup> Future work should focus on porting known design strategies from established OMIECs, such as synthesizing more hydrophilic 2DPs through side chain modification.<sup>[14,18]</sup>

These results show that the 2DP TIIP can be polymerized and patterned to achieve a micrometer-scale operational transistor with respectable mobilities of  $0.05 \text{ cm}^2 \text{ V}^{-1} \text{ s}^{-1}$ . While this value is approximately two orders of magnitude lower than the highest performance conjugated linear polymers, macroscale measurements of 2DP semiconductor performance are an important step toward evaluating the potential of macromolecular sheets as semiconductors, which have been shown to have high mobilities through nanoscale spectroscopy measurements and density functional theory calculations.<sup>[32,33,46–49]</sup>

Demonstrated 2DP-based OECT fabrication and device performance foreshadows a new OMIEC design paradigm. Now that 2DP-based OECT performance has been established, it will be more straightforward to explore the systematic optimization of these materials for OECTs. However, at present, the performance of these devices falls short of their potential. Presumably, the discontinuous, defect-prone films that are presently available limit the potential of 2DPs as semiconductors. Undeniably, hydrophobicity, defect prevalence, mesoscale ordering, and macroscale morphology will influence ionic injection, electrolyte transport, and long-range electronic mobilities. While we observe direct evidence for bulk film charging in this work, it is unclear whether this ion injection occurs via defects or through the designed porosity of the framework. In line with this question is whether the charging observed is limited to defect/amorphous regions interfacing with crystalline 2DPs domains (as is the case with alkylated conjugated polymer:polymer electrolyte blend OMIECs, or some nanofibrillar materials), or if charge-carrier distribution is more uniform throughout the bulk. Future investigations into molecular design and film formation/processing will answer these questions and allow for rapid iteration in 2DP development as active materials for OECTs and other microelectronic components.

### 3. Conclusion

We have demonstrated that a two-dimensional polymer, TIIP, can be polymerized, patterned, and operated as a micrometer-scale electrochemical transistor. TIIP films were deposited by direct polymerization, followed by dry PaC liftoff, which produced devices with well-defined channel dimensions. The device shows low hysteresis operation and bulk modulation of channel conductance, consistent with OECT operation. The measured electrical characteristics reveal a charging of  $0.8 \text{ mF cm}^{-2}$ , approximated as  $32 \text{ F cm}^{-3}$  for volumetric capacitance, with a hole mobility of  $0.05 \text{ cm}^2 \text{ V}^{-1} \text{ s}^{-1}$ .

These findings show that 2DPs are a viable and distinct new class of OECT active layers. The ideal OMIEC design calls for

an anisotropic material where ionic injection and transport are orthogonal to the transistor channel and electronic transport occurs within the plane of the channel, bridging a source and drain electrode. Semiconducting 2DPs nominally meet these requirements extremely well. Because the 2DP backbone (and thus the electronic structure) and pore functionality are orthogonal and can be aligned, it should be possible to systematically engineer OMIECs with tailored conductivities, capacitances, response times, and selectivity. As these synthetic design parameters are uncovered, we anticipate that 2DP transistors will also be optimized for applications such as chemical sensing or neuromorphic computing. To realize this development, it will be critical to understand and control the microscale structure of 2DPs including their domain size, defect density, and grain boundaries. Specifically, we expect that the polycrystalline nature of 2DPs is more susceptible to disrupted inter-grain transport during electrochemical cycling, which may contribute to the limited stability of these OECT devices. While this study does not address these challenges in full, it is a proof-of-principle demonstration that maturing synthetic and fabrication techniques are reaching the required fidelity to enable these explorations.

### Supporting Information

Supporting Information is available from the Wiley Online Library or from the author.

### Acknowledgements

R.B.R., A.M.E. contributed equally to this work. J.R. and R.B.R gratefully acknowledge support from the Alfred P. Sloan Foundation (FG-2019-12046). W.R.D. and S.R.M. gratefully acknowledge support by the United States Army Research Office for a Multidisciplinary University Research Initiative (MURI) award (W911NF-15-1-0447). The authors thank X. Ji (Northwestern) for fruitful discussion and support on figure composition. This work utilized the Northwestern University Micro/Nano Fabrication Facility (NUFAB), which is partially supported by Soft and Hybrid Nanotechnology Experimental (SHyNE) Resource (NSF ECCS-1542205), the Materials Research Science and Engineering Center (DMR-1720139), the State of Illinois, and Northwestern University. This work made use of the Keck-II facilities of Northwestern University's NUANCE Center, which had received support from the Soft and Hybrid Nanotechnology Experimental (SHyNE) Resource (NSF ECCS-1542205); the MRSEC program (NSF DMR-1720139) at the Materials Research Center; the International Institute for Nanotechnology (IIN); the Keck Foundation; and the State of Illinois, through the IIN. A.M.E. is supported by the National Science Foundation Graduate Research Fellowship (DGE-1324585). This research used resources of the Advanced Photon Source (Sectors 8) a U.S. Department of Energy (DOE) Office of Science User Facility operated for the DOE Office of Science by Argonne National Laboratory under Contract No. DE-AC02-06CH11357. The authors acknowledge Gatan Inc., Pleasanton, CA, USA, for the use of the K3-IS camera installed at the EPIC facility of Northwestern University's NUANCE Center. Research reported in this publication was supported in part by instrumentation provided by the Office of The Director, National Institutes of Health of the National Institutes of Health under Award Number S10OD026871. The content is solely the responsibility of the authors and does not necessarily represent the official views of the National Institutes of Health. This work made use of the EPIC facility of Northwestern University's NUANCE Center, which has received support from the SHyNE Resource (NSF ECCS-2025633), the IIN, and Northwestern's MRSEC program (NSF DMR-1720139).

## Conflict of Interest

The authors declare no conflict of interest.

## Data Availability Statement

The data that support the findings of this study are available from the corresponding author upon reasonable request.

## Keywords

2D polymers, covalent organic frameworks, thin-film transistors, organic electrochemical transistors

Received: December 31, 2021

Revised: February 28, 2022

Published online: April 21, 2022

- [1] J. Rivnay, S. Inal, A. Salleo, R. M. Owens, M. Berggren, G. G. Malliaras, *Nat. Rev. Mater.* **2018**, *3*, 17086.
- [2] X. Strakosas, M. Bongo, R. M. Owens, *J. Appl. Polym. Sci.* **2015**, 132.
- [3] D. Khodagholy, J. Rivnay, M. Sessolo, M. Gurfinkel, P. Leleux, L. H. Jimison, E. Stavrinidou, T. Herve, S. Sanaur, R. M. Owens, G. G. Malliaras, *Nat. Commun.* **2013**, *4*, 2133.
- [4] A. M. Pappa, D. Ohayon, A. Giovannitti, I. P. Maria, A. Savva, I. Uguz, J. Rivnay, I. McCulloch, R. M. Owens, S. Inal, *Sci. Adv.* **2018**, *4*, eaat0911.
- [5] M. Braendlein, A. M. Pappa, M. Ferro, A. Lopresti, C. Acquaviva, E. Mamessier, G. G. Malliaras, R. M. Owens, *Adv. Mater.* **2017**, *29*, 1605744.
- [6] P. Gkoupidenis, N. Schaefer, B. Garlan, G. G. Malliaras, *Adv. Mater.* **2015**, *27*, 7176.
- [7] Y. van de Burgt, E. Lubberman, E. J. Fuller, S. T. Keene, G. C. Faria, S. Agarwal, M. J. Marinella, A. A. Talin, A. Salleo, *Nat. Mater.* **2017**, *16*, 414.
- [8] J. T. Friedlein, R. R. McLeod, J. Rivnay, *Org. Electron.* **2018**, *63*, 398.
- [9] A. Giovannitti, R. B. Rashid, Q. Thiburce, B. D. Paulsen, C. Cendra, K. Thorley, D. Moia, J. T. Mefford, D. Hanifi, D. Weiyuan, M. Moser, A. Salleo, J. Nelson, I. McCulloch, J. Rivnay, *Adv. Mater.* **2020**, *32*, 1908047.
- [10] B. D. Paulsen, S. Fabiano, J. Rivnay, *Annu. Rev. Mater. Res.* **2021**, *51*, 73.
- [11] B. D. Paulsen, K. Tybrandt, E. Stavrinidou, J. Rivnay, *Nat. Mater.* **2020**, *19*, 13.
- [12] A. Giovannitti, D.-T. Sbircea, S. Inal, C. B. Nielsen, E. Bandiello, D. A. Hanifi, M. Sessolo, G. G. Malliaras, I. McCulloch, J. Rivnay, *Proc. Natl. Acad. Sci. USA* **2016**, *113*, 12017.
- [13] C. B. Nielsen, A. Giovannitti, D.-T. Sbircea, E. Bandiello, M. R. Niazi, D. A. Hanifi, M. Sessolo, A. Amassian, G. G. Malliaras, J. Rivnay, *J. Am. Chem. Soc.* **2016**, *138*, 10252.
- [14] Z. S. Parr, R. B. Rashid, B. D. Paulsen, B. Poggi, E. Tan, M. Freeley, M. Palma, I. Abrahams, J. Rivnay, C. B. Nielsen, *Adv. Electron. Mater.* **2020**, *6*, 2000215.
- [15] X. Chen, A. Marks, B. D. Paulsen, R. Wu, R. B. Rashid, H. Chen, M. Alsufyani, J. Rivnay, I. McCulloch, *Angew. Chem., Int. Ed.* **2021**, *60*, 9368.
- [16] A. Giovannitti, C. B. Nielsen, D.-T. Sbircea, S. Inal, M. Donahue, M. R. Niazi, D. A. Hanifi, A. Amassian, G. G. Malliaras, J. Rivnay, I. McCulloch, *Nat. Commun.* **2016**, *7*, 13066.
- [17] D. Ohayon, A. Savva, W. Du, B. D. Paulsen, I. Uguz, R. S. Ashraf, J. Rivnay, I. McCulloch, S. Inal, *ACS Appl. Mater. Interfaces* **2021**, *13*, 4253.
- [18] C. G. Bischak, L. Q. Flagg, K. Yan, C.-Z. Li, D. S. Ginger, *ACS Appl. Mater. Interfaces* **2019**, *11*, 28138.
- [19] I. P. Maria, B. D. Paulsen, A. Savva, D. Ohayon, R. Wu, R. Hallani, A. Basu, W. Du, T. D. Anthopoulos, S. Inal, J. Rivnay, I. McCulloch, A. Giovannitti, *Adv. Funct. Mater.* **2021**, *31*, 2008718.
- [20] S. Inal, G. G. Malliaras, J. Rivnay, *Nat. Commun.* **2017**, *8*, 1767.
- [21] H. B. Balch, A. M. Evans, R. R. Dasari, H. Li, R. Li, S. Thomas, D. Wang, R. P. Bisbey, K. Slicker, I. Castano, S. R. Xun, L. Jiang, C. Zhu, N. Gianneschi, D. C. Ralph, J.-L. Brédas, S. R. Marder, W. R. Dichtel, F. Wang, *J. Am. Chem. Soc.* **2020**, *142*, 21131.
- [22] A. Savva, R. Hallani, C. Cendra, J. Surgailis, T. C. Hidalgo, S. Wustoni, R. Sheelamanthula, X. Chen, M. Kirkus, A. Giovannitti, A. Salleo, I. McCulloch, S. Inal, *Adv. Funct. Mater.* **2020**, *30*, 1907657.
- [23] R. Giridharagopal, L. Flagg, J. Harrison, M. Ziffer, J. Onorato, C. Luscombe, D. Ginger, *Nat. Mater.* **2017**, *16*, 737.
- [24] L. Q. Flagg, C. G. Bischak, J. W. Onorato, R. B. Rashid, C. K. Luscombe, D. S. Ginger, *J. Am. Chem. Soc.* **2019**, *141*, 4345.
- [25] B. D. Paulsen, R. Wu, C. Takacs, H.-G. Steinrück, J. Strzalka, Q. Zhang, M. F. Toney, J. Rivnay, *Adv. Mater.* **2020**, *32*, 2003404.
- [26] P. J. Flory, J. Rehner jr., *J. Chem. Phys.* **1943**, *11*, 512.
- [27] N. Huang, P. Wang, D. Jiang, *Nat. Rev. Mater.* **2016**, *1*, 16068.
- [28] A. M. Evans, N. P. Bradshaw, B. Litchfield, M. J. Strauss, B. Seckman, M. R. Ryder, I. Castano, C. Gilmore, N. C. Gianneschi, C. R. Mulzer, M. C. Hersam, W. R. Dichtel, *Adv. Mater.* **2020**, *32*, 2004205.
- [29] D. Burmeister, M. G. Trunk, M. J. Bojdys, *Chem. Soc. Rev.* **2021**, *50*, 11559.
- [30] B. Sun, C.-H. Zhu, Y. Liu, C. Wang, L.-J. Wan, D. Wang, *Chem. Mater.* **2017**, *29*, 4367.
- [31] J. M. Rotter, R. Guntermann, M. Auth, A. Mähringer, A. Sperlich, V. Dyakonov, D. D. Medina, T. Bein, *Chem. Sci.* **2020**, *11*, 12843.
- [32] E. Jin, M. Asada, Q. Xu, S. Dalapati, M. A. Addicoat, M. A. Brady, H. Xu, T. Nakamura, T. Heine, Q. Chen, D. Jiang, *Science* **2017**, *357*, 673.
- [33] S. Thomas, H. Li, R. R. Dasari, A. M. Evans, I. Castano, T. G. Allen, O. G. Reid, G. Rumbles, W. R. Dichtel, N. C. Gianneschi, S. R. Marder, V. Coropceanu, J. L. Brédas, *Mater. Horiz.* **2019**, *6*, 1868.
- [34] Y. Zhong, B. Cheng, C. Park, A. Ray, S. Brown, F. Mujid, J.-U. Lee, H. Zhou, J. Suh, K.-H. Lee, A. J. Mannix, K. Kang, S. J. Sibener, D. A. Muller, J. Park, *Science* **2019**, *366*, 1379.
- [35] A. M. Evans, A. Giri, V. K. Sangwan, S. Xun, M. Bartnof, C. G. Torres-Castanedo, H. B. Balch, M. S. Rahn, N. P. Bradshaw, E. Vitaku, D. W. Burke, H. Li, M. J. Bedzyk, F. Wang, J. L. Brédas, J. A. Malen, A. J. H. McGaughey, M. C. Hersam, W. R. Dichtel, P. E. Hopkins, *Nat. Mater.* **2021**, *20*, 1142.
- [36] H. Sahabudeen, H. Qi, M. Ballabio, M. Položij, S. Olthof, R. Shivhare, Y. Jing, S. Park, K. Liu, T. Zhang, J. Ma, B. Rellinghaus, S. Mannsfeld, T. Heine, M. Bonn, E. Cánovas, Z. Zheng, U. Kaiser, R. Dong, X. Feng, *Angew. Chem., Int. Ed.* **2020**, *59*, 6028.
- [37] K. Liu, H. Qi, R. Dong, R. Shivhare, M. Addicoat, T. Zhang, H. Sahabudeen, T. Heine, S. Mannsfeld, U. Kaiser, Z. Zheng, X. Feng, *Nat. Chem.* **2019**, *11*, 994.
- [38] V. Müller, A. Hinaut, M. Moradi, M. Baljovic, T. A. Jung, P. Shahgaldian, H. Möhwald, G. Hofer, M. Kröger, B. T. King, E. Meyer, T. Glatzel, D. Schlüter, *Angew. Chem., Int. Ed.* **2018**, *57*, 10584.
- [39] D. Zhou, X. Tan, H. Wu, L. Tian, M. Li, *Angew. Chem.* **2019**, *131*, 1390.
- [40] J. Rivnay, P. Leleux, M. Ferro, M. Sessolo, A. Williamson, D. A. Koutsouras, D. Khodagholy, M. Ramuz, X. Strakosas, R. M. Owens, C. Benar, J.-M. Badiet, C. Bernard, G. G. Malliaras, *Sci. Adv.* **2015**, *1*, e1400251.

- [41] D. Khodagholy, T. Doublet, M. Gurfinkel, P. Quilichini, E. Ismailova, P. Leleux, T. Herve, S. Sanaur, C. Bernard, G. G. Malliaras, *Adv. Mater.* **2011**, *23*, H268.
- [42] C. R. Mulzer, L. Shen, R. P. Bisbey, J. R. McKone, N. Zhang, H. c. D. Abruña, W. R. Dichtel, *ACS Cent. Sci.* **2016**, *2*, 667.
- [43] J. Bisquert, G. Garcia-Belmonte, F. Fabregat-Santiago, A. Compte, *Electrochem. Commun.* **1999**, *1*, 429.
- [44] P. R. Paudel, J. Tropp, V. Kaphle, J. D. Azoulay, B. Lüssem, *J. Mater. Chem. C* **2021**.
- [45] C. M. Proctor, J. Rivnay, G. G. Malliaras, *Polym. Phys.* **2016**, *54*, 1433.
- [46] N. C. Flanders, M. S. Kirschner, P. Kim, T. J. Fauvell, A. M. Evans, W. Helweh, A. P. Spencer, R. D. Schaller, W. R. Dichtel, L. X. Chen, *J. Am. Chem. Soc.* **2020**, *142*, 14957.
- [47] X. Feng, L. Liu, Y. Honsho, A. Saeki, S. Seki, S. Irle, Y. Dong, A. Nagai, D. Jiang, *Angew. Chem.* **2012**, *124*, 2672.
- [48] X. Ding, L. Chen, Y. Honsho, X. Feng, O. Saengsawang, J. Guo, A. Saeki, S. Seki, S. Irle, S. Nagase, V. Parasuk, D. Jiang, *J. Am. Chem. Soc.* **2011**, *133*, 14510.
- [49] X. Ding, J. Guo, X. Feng, Y. Honsho, J. Guo, S. Seki, P. Maitarad, A. Saeki, S. Nagase, D. Jiang, *Angew. Chem., Int. Ed.* **2011**, *50*, 1289.